ARTICLES

CF_2Cl_2 Decomposition over Nanocrystalline MgO: Evidence for Long Induction Periods

Ilya V. Mishakov,[†] Vladimir I. Zaikovskii,[†] David S. Heroux,[†,‡] Alexander F. Bedilo,*[,‡] Vladimir V. Chesnokov,[†] Alexander M. Volodin,[†] Igor N. Martyanov,[‡] Svetlana V. Filimonova,[†] Valentin N. Parmon,[†] and Kenneth J. Klabunde[‡]

Boreskov Institute of Catalysis, Novosibirsk, Russia, 630090, and Department of Chemistry, Kansas State University, Manhattan, Kansas 66506

Received: May 19, 2004; In Final Form: December 28, 2004

CF_2Cl_2 has been found to react with nanoscale MgO at 325 °C and higher temperatures. In excess of the halocarbon, the reaction results in the formation of MgF_2 as a predominant solid product, with CCl_4, and CO_2 formed as the main gaseous products. The kinetics of the process is characterized by a prolonged induction period, which is as long as 8.5 h at 325 °C. The length of the induction period decreases with temperature increase and becomes negligible at 500 °C. Complete CF_2Cl_2 mineralization has been achieved in an excess of MgO at 450 °C. Detailed HRTEM and EDX analysis has shown that the induction period involves the formation of small amounts of magnesium halides on the oxide surface and results in its reconstruction leading to initial oriental ordering of the nanocrystals followed by substantial changes in the bulk composition of the nanoparticles. The reaction proved to be structurally sensitive. It has been found that deep fluoridation is possible only for nanoscale MgO samples. The use of samples with lower surface areas results in lengthening of the induction period and decrease of the reaction depth. The MgO transformation to MgF_2 has been found to result in a surface area decrease by more that an order of magnitude as a result of intense sintering of magnesium fluoride under the reaction conditions.

Introduction

Chlorofluorocarbons present a hazard to the environment because of their ability to destroy the ozone layer. Since CFCs are very stable molecules, they are hard to destroy and can persist in the atmosphere for long periods of time.[1] In the atmosphere, UV light is able to break the C−Cl bond of the CFC and generate chlorine radicals. The mechanism discovered by Rowland and Molina shows that the Cl radical can be regenerated and can react further with another ozone molecule.[2]

Many methods have been studied in the destruction of CFCs. Mostly, studies have been conducted on metal oxides for use in catalytic hydrolysis.[3−5] The disadvantage of this method is that HF and HCl are produced in the reaction. Therefore, this requires a system to neutralize the produced gases and a special noncorrosive reactor.

For the past decade, nanoscale alkaline earth metal oxides have attracted significant attention as effective sorbents of various toxic compounds. Destructive sorption of flue gases,[6−8] toxic organo-phosphorus compounds,[9−12] and chlorinated hydrocarbons[13−17] has been studied over aerogel-prepared (AP) MgO and CaO. It has been shown that chlorine atoms are substituted for lattice oxygen following a multistage mechanism, with phosgene serving as an intermediate. Destructive sorption of CCl_4 over AP-MgO and AP-CaO promoted with iron and vanadium oxide has also been investigated.[15−17] The transition metal oxide proved to work as a catalyst intermediate increasing the mobility of ions in the solid and moving O^{2-} ions to CCl_4 with simultaneous transition of Cl^- ions to the oxide.

CCl_3F and CCl_2F_2 destructive adsorption has been studied over modified MgO, particularly with vanadium.[18,19] Tamai recently published that CCl_2F_2 did not show any reaction with MgO below 450 °C.[19]

The most interesting feature of aerogel-prepared materials is their extremely high dispersity leading to unusually high surface area for alkaline earth metal oxides (up to 500 m^2/g for AP-MgO).[8] Such a high surface area is achieved due to the use of a sol−gel technique involving hydrolysis of metal alkoxides in organic solvents followed by drying under supercritical conditions for their synthesis. Due to their high surface area and unusual crystal shape, these materials have unusually high concentrations of low-coordinated metal and oxygen ions on their surface[20] that bring unique sorption properties.

The nanocrystals in such oxide materials are often as small as 2−3 nm. In practice, this makes their whole volume as reactive as the surface and near-surface areas of common microcrystalline materials. Naturally, such materials are ideally suited for application as bulk chemisorbents with high reactivity and adsorption capacity in processes where destruction of gaseous compounds may be due not only to their adsorption on the surface but also to chemical transformation of the bulk solid material itself.

In the present paper, we report the first evidence of the destructive adsorption of CF_2Cl_2 at lower temperatures as well

* Corresponding author. E-mail: abedilo@bk.ru.
[†] Boreskov Institute of Catalysis.
[‡] Department of Chemistry, Kansas State University.

10.1021/jp047847s CCC: $30.25 © 2005 American Chemical Society
Published on Web 03/30/2005

as a detailed analysis of the chemical and structural transformations of AP-MgO needed for the reaction to take place.

Experimental Section

Three different MgO samples were used in the experiments. AP-MgO with the surface area of 385 m^2/g was prepared by a sol−gel technique involving high-temperature supercritical drying described in detail earlier.[8,21] CP-MgO (281 m^2/g) was obtained by decomposition of $Mg(OH)_2$ prepared by hydration of commercial MgO.[3] In both cases, the final preparation step was overnight evacuation at 500 °C. Then, the samples were stored under ambient conditions. Their performance was compared to that of a commercial low-surface-area sample CM-MgO (10 m^2/g).

CF_2Cl_2 of "pure" grade and Ar of "ultrapure" grade were used in the experiments. In the latter case, the argon content was no less that 99.99%, with oxygen concentration less than 0.001 vol % and water vapor amount less than 0.1 g/ m^3.

A flow reactor equipped with a MacBain balance and an on-line gas chromatograph was used in the flow experiments. This made it possible to monitor both the composition of the products and the sample weight during the reaction. The sensitivity in the determination of the sample weight was 10^{-4} g. CF_2Cl_2 was passed through the reactor with a volume rate of 3 L/h. MgO sample weight was 0.05−0.1 g. Unless otherwise stated, the samples were activated in Ar flow at 500 °C for 30 min. Samples during the induction period were obtained by stopping the flow of CCl_2F_2 at the desired time and purging the reactor with Ar.

High-resolution transmission electron microscopy (HTREM) was performed using a JEOL JEM-2010 instrument with lattice resolution 1.4 Å and accelerating voltage 200 kV. Selected area diffraction (SAD) was used for the phase identification. Samples for microscopy were prepared by suspending the powders in ethanol, followed by ultrasound treatment (5 W/cm^2). Then, an aerosol created from the suspension was deposited on thin supports. Holey amorphous carbon films with the thickness of 10−20 nm supported on standard copper grids were used as the supports.

Local elemental analysis was performed using a JEM-2010 instrument with an EDAX energy-dispersive X-ray Phoenix spectrometer equipped with a Si(Li) detector with energy resolution 130 eV.

Static volume experiments were performed in a vacuum installation under reduced pressure. In a typical experiment, an AP-MgO sample (0.04 g, 10^{-3} mol) was placed in a 200-mL two-neck Schlenk tube and evacuated at 500 °C for 2 h. Then, the sample was cooled to 340 °C and approximately 240 Torr CF_2Cl_2 was introduced. As the temperature varied along the length of the tube, additional calibration was performed to determine the amount of the gas introduced, which was estimated to be about 2×10^{-3} mol. Several experiments at other temperatures and gas pressures were also performed. A small amount of xenon was used as an internal standard. The second neck of the tube was sealed with a septum and used for sampling. The products were analyzed using a Shimadzu GCMS-QP5000 gas chromatograph mass spectrometer equipped with a 30-m Restec capillary column with XTI-5 phase.

Specific surface areas of the samples were determined by the BET method using thermal desorption of argon.

XRD studies were performed using a Siemens D-500 instrument with Cu Kα monochromatic irradiation (graphite monochromator on reflected beam). Silicon powder was used as an internal standard.

^{19}F NMR experiments were carried out using a Bruker MSL-400 Fourier transform pulse NMR spectrometer at 396.5 MHz frequency with a pulse width of 0.7 μs and a 30-s delay between pulses. The chemical shifts were measured with respect to hexafluorobenzene used as an external standard. Low field shifts were considered as positive. Depending on the signal-to-noise ratio, 25−2000 scans were accumulated over the 300-kHz spectral range.

FTIR spectra in the range of 500−4000 cm^{-1} were registered using a Mattson Research Series-1 spectrometer. The experiments were performed in a stainless steel in situ FTIR cell similar to the one described by Yates et al.[22] A detailed description of the installation used in the FTIR experiments can be found elsewhere.[23] MgO powder was pressed onto half of a tungsten grid. The other half of the grid was used for collecting background spectra. First, the sample was activated under vacuum at 500 °C for 2 h. Then, it was cooled to 350 °C, and 15 Torr CF_2Cl_2 was introduced. A typical MgO/CF_2Cl_2 molar ratio was approximately 1:1.5. The spectra of the sample with gas phase were recorded each 10 min for 1.5 h without moving the cell. A separate experiment was performed in order to distinguish the contribution of the gas phase from that of the adsorbed forms.

Results and Discussion

1. Thermodynamic Analysis of CF_2Cl_2 Reaction with MgO. CF_2Cl_2 is a colorless and odorless gas, which is chemically very inert and has a high thermal stability. First, we evaluated the feasibility of its possible reactions with MgO in a broad temperature range from the thermodynamic standpoint. One can imagine five main possible routes for the CF_2Cl_2 reaction with MgO resulting in significantly different product compositions. Although the formation of magnesium oxyhalides as reaction intermediates is also possible, they are not very stable, and, thus, will not be discussed in the thermodynamic section. The reactions listed below were normalized to the same amount of MgO.

$$2MgO + CF_2Cl_2 \rightarrow MgF_2 + MgCl_2 + CO_2 \quad (1)$$

$$2MgO + 2CF_2Cl_2 \rightarrow 2MgF_2 + 2COCl_2 \quad (2)$$

$$2MgO + 2CF_2Cl_2 \rightarrow 2MgCl_2 + 2COF_2 \quad (3)$$

$$2MgO + 2CF_2Cl_2 \rightarrow 2MgF_2 + CO_2 + CCl_4 \quad (4)$$

$$2MgO + 2CF_2Cl_2 \rightarrow 2MgCl_2 + CO_2 + CF_4 \quad (5)$$

In principle, either of the halide atoms or both of them can be bonded to magnesium in the final product. If only one of the magnesium halides is selectively formed, resulting carbon oxohalides can be imagined to disproportionate to CO_2 and the corresponding carbon tetrahalide, which are very stable products. Note that the compositions of both the gas and the solid phases should be different in these cases.

Figure 1 proves that all suggested reactions are thermodynamically feasible in the whole temperature range. Reactions leading to the formation of magnesium fluoride are more favorable thermodynamically, whereas the formation of magnesium chloride is less probable from the thermodynamic point of view as a result of a significant difference in the energies of Mg−F and Mg−Cl bonds (121 and 91 kcal/mol, respectively). The formation of stable products (CO_2, CCl_4, and CF_4) is also more favorable thermodynamically in comparison with $COCl_2$

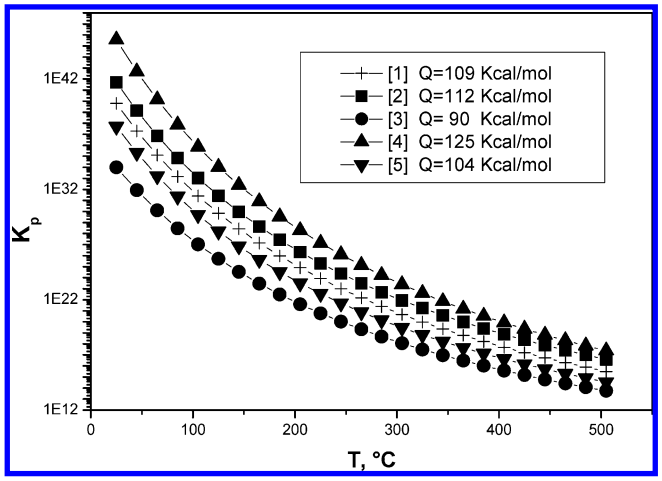

Figure 1. Temperature dependence of the equilibrium constant for possible reactions of MgO with CF_2Cl_2. Numbers in parentheses correspond to reaction numbers in the text.

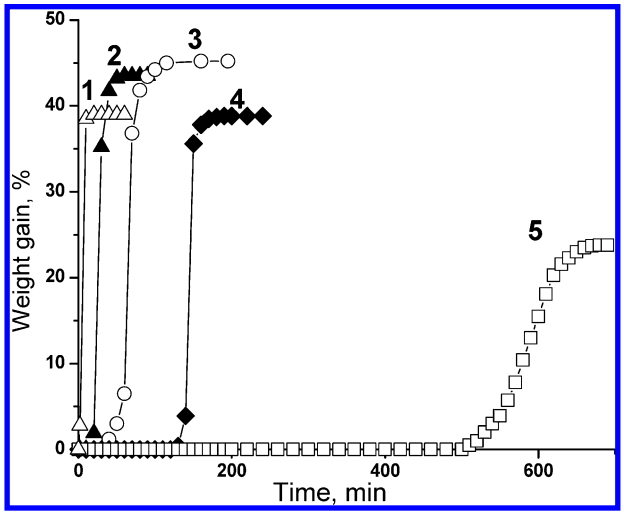

Figure 2. Kinetic curves of the weight gain of AP-MgO treated with CF_2Cl_2 at 500 (1), 450 (2), 400 (3), 350 (4), and 325 °C (5).

and COF_2. The latter two compounds may be expected to form only in minor amounts as intermediates.

As a result, reaction 4 appears to be the most likely when normalized to the amount of MgO. This situation is implemented in excess of the halocarbon. On the other hand, in excess of MgO reactions should be normalized to the same amount of the halocarbon. This would make reaction 1 resulting in simultaneous formation of both magnesium halides a clear winner, since energies of all other reactions should be divided by a factor of 2. Hence, one can expect the formation of different reaction products depending on which of the reactants is taken in excess.

2. Kinetics of AP-MgO Reaction with CF_2Cl_2: Discovery of the Induction Period. CF_2Cl_2 appeared to react with nanoscale MgO at temperatures as low as 325 °C to give a significant gain of the sample weight, as evidenced by kinetic curves presented in Figure 2. The presence of an obvious induction period, after which an intense gain of the sample weight starts, is the most distinctive and interesting feature of the kinetic curves. The duration of the induction period depends on the reaction temperature. At 350 °C it exceeds 2 h (curve 4), while at 500 °C the sample weight gain starts almost immediately (curve 1). The induction period becomes more than 8.5-h long when the reaction temperature is further decreased to 325 °C (curve 5). The induction period phenomenon is

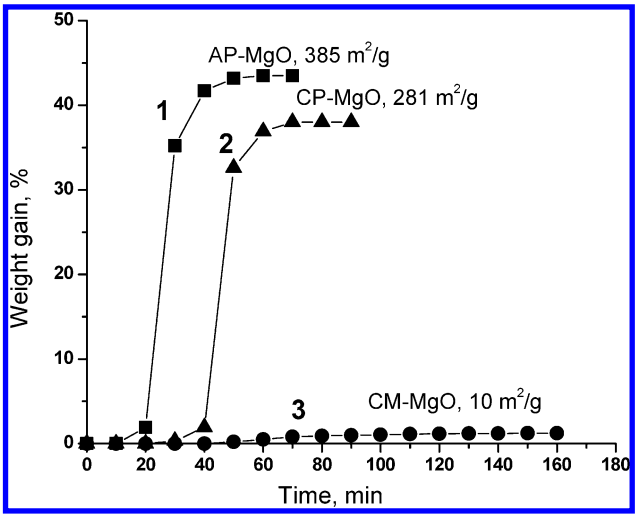

Figure 3. Weight gain of different MgO samples during their treatment with CF_2Cl_2 at 450 °C. 1: AP-MgO (385 m^2/g), 2: CP-MgO (281 m^2/g), 3: CM-MgO (10 m^2/g).

reproduced with 100% probability, and its duration is reproduced with appropximately 5−10% accuracy when all conditions are kept the same.

The existence of an induction period on the kinetic curve must be connected with a gradual accumulation of certain active sites or defects on the MgO surface, which eventually lead to complete transformation of the nanoparticles. As soon as enough active sites are accumulated, intense bulk substitution of oxygen by fluorine starts. At lower temperatures, the rate of the halocarbon reaction with the oxide surface is significantly lower. This makes the induction period much longer. Note that the weight gain stops at values close to 40−45%, indicating the end of the reaction. The maximum theoretical weight gain corresponding to complete transformation of the oxide to fluoride is 55%. This indicates that about 80% transformation is actually achieved in our experiments.

To evaluate the role of the small crystals of AP-MgO in the reaction with CF_2Cl_2, similar experiments were performed over other MgO samples prepared by different methods, having lower surface areas and different crystal sizes and shapes.[8,20] An experiment with CP-MgO (Figure 3, curve 2) showed that the induction period was longer over the sample with the lower surface area and that the maximum MgO conversion to MgF_2 was lower. The kinetics of the process proved to be very different over CM-MgO, which had a surface area 40 times lower than that of AP-MgO. As shown in Figure 3, CM-MgO barely reacts with CF_2Cl_2, giving the weight gain of only 1.5%. Thus, the dispersity and crystalline nature of the samples appear to have a decisive effect on the rate and depth of the MgO reaction with CF_2Cl_2 leading to the formation of the MgF_2 phase.

The surface of AP-MgO is known to contain some adsorbed water before activation at elevated temperatures. Significant amounts of hydroxyl groups partially covering the surface are usually present, even after activation at 500 °C under vacuum.[8] Plus, the structure of the AP-MgO surface can be changed significantly during prolonged storage, and it can be partially converted back to hydroxide due to the reaction with the atmospheric moisture.

To reveal the effect of water present on the surface of AP-MgO on the induction period, we have performed a similar experiment starting with AP-$Mg(OH)_2$. In this comparative experiment, AP-$Mg(OH)_2$ was subjected to heat treatment in argon at 500 °C until complete transformation to magnesium oxide, followed by the reaction with CF_2Cl_2 at 400 °C. Figure

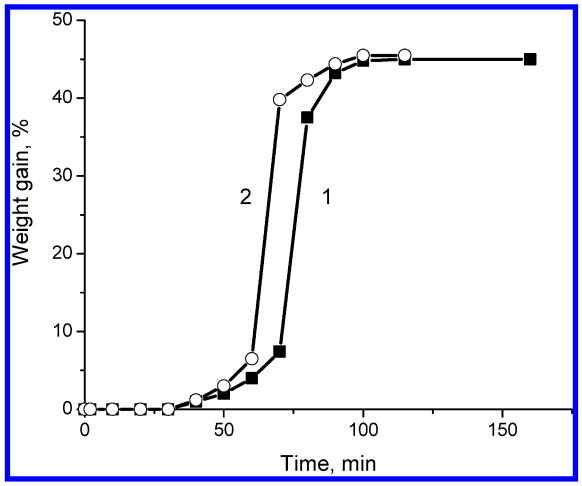

Figure 4. Kinetic curves of the weight gain of AP-MgO (1) and AP-MgO prepared by in-situ decomposition of $Mg(OH)_2$ (2) during reaction with CF_2Cl_2 at 400 °C.

4 shows that the kinetic curves corresponding to AP-MgO used in other experiments (curve 1) and AP-MgO prepared from hydroxide in situ (curve 2) are nearly identical. So, the presence of the induction period on the kinetic curve does not depend on whether a freshly prepared or "aged" AP-MgO is used in the experiment.

3. Induction Period Analysis. *(a) EDX and TEM Studies.* Energy-dispersive X-ray (EDX) spectroscopy in combination with HRTEM allowed us to simultaneously monitor the changes in the elemental composition and morphology during the induction period and characterize the individual particles formed after the reaction.

Figure 5 shows the TEM images of AP-MgO at different stages of reaction with CF_2Cl_2. The sample before the reaction with CCl_2F_2 (Figure 5A) consists of curved flat whiskers of sizes, $l \sim 30-50$ nm, $h \sim 5$ nm, which are composed of chains of cubic MgO nanocrystals 2−3 nm in sizes (Figure 6A). This is consistent with previous HRTEM studies of AP-MgO.[21,24]

A low-magnification TEM image of a sample after half of the induction period for the reaction of CCl_2F_2 with AP-MgO at 400 °C is shown in Figure 5B. The whiskerlike structures of the agglomerates have condensed greatly, so that the large pores present in the initial MgO are no longer present in this sample. The HRTEM image in Figure 6B shows that after half of the induction period the nanocrystals are packed much more densely but are mostly of the same size as in the starting MgO. However, some of the nanocrystallites have sintered to form ordered crystallites on the order of 10 nm (see arrows).

The low- and high-magnification TEM images of the sample very near the end of the induction period during the reaction are shown in Figures 5C and 6C, respectively. This sample was obtained after 40 min of reaction at 400 °C. The beginning of the rapid conversion to MgF_2 begins near 55 min. After 40 min on stream, the CCl_2F_2 was stopped and rapidly purged with argon. This sample had a weight increase of ∼0.4%. Both images show that this sample consists of dense clusters with large, well-ordered crystallites that are much larger than the nanocrystals of the starting material (compare images A and C in Figure 6).

Table 1 shows the EDX data for the samples during the induction period. The EDX spectra were obtained for samples after 20 min, which is close to one-half of the induction period, and after 40 min, which is near the end of the induction period. Two different analyses were obtained for each sample: a wide electron beam analysis, ∼1000 nm, which indicates average

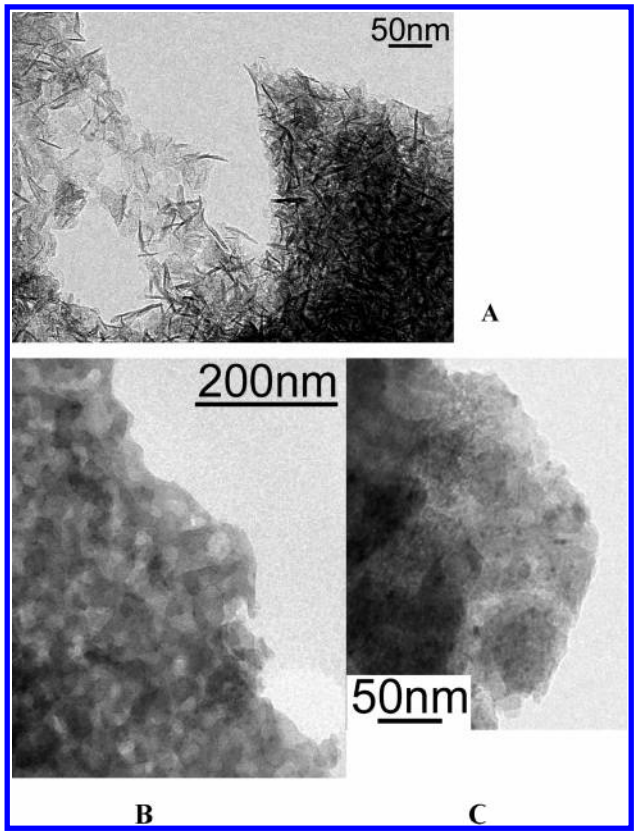

Figure 5. TEM images of AP-MgO: (A) before the reaction with CCl_2F_2; (B) after 20 min, approximately the halfway point of the induction period; (C) after 40 min, near the end of the induction period.

values for the elemental ratios, and a narrow beam analysis, 25 nm, which focuses on the surface composition of the particles.

The EDX results indicate that initially both chlorine and fluorine are incorporated into MgO in comparable amounts, whereas the surface is enriched with fluorine (compare wide and narrow beam samples after 20 min on stream). As time goes on, the concentration of fluorine increases considerably, whereas that of chlorine does not change much. The TEM and EDX data show that the chlorine is not observed as crystalline $MgCl_2$ and, probably, forms only strongly adsorbed species and defective oxyhalide structures with variable amounts of halogen atoms partially substituting oxygen atoms of MgO. Apparently, the substitution of chlorine with fluorine results in the formation of minor amounts of small MgF_2 crystals. These conclusions are supported by the narrow beam data for the sample after 40 min. Here it is seen that after exposure to the high vacuum of the TEM, very little Cl is present near the surface of the crystals, but a high F/Mg ratio is observed.

The TEM image of the sample taken from the reactor after the weight gain during the reaction with CCl_2F_2 stopped is presented in Figure 7. It shows that the sample consists of particles of two very different morphologies. First, large irregular particles ranging from 100 to 300 nm in size, and, second, clusters of small relatively uniform particles about 50 nm in size are present throughout the sample. The XRD studies of these materials showed the presence of both MgF_2 and some MgO (Figure 8A). It may be expected that this was the result of MgO cores in larger particles due to limited diffusion into the particle. EDX data has shown this not to be the case.

Figure 9 shows the EDX spectra from the clusters of 50-nm particles (a) and from the larger particles (b). The analysis of the cluster of particles ∼50 nm in size shows that they are still mostly MgO that is only partially converted to MgF_2. Surpris-

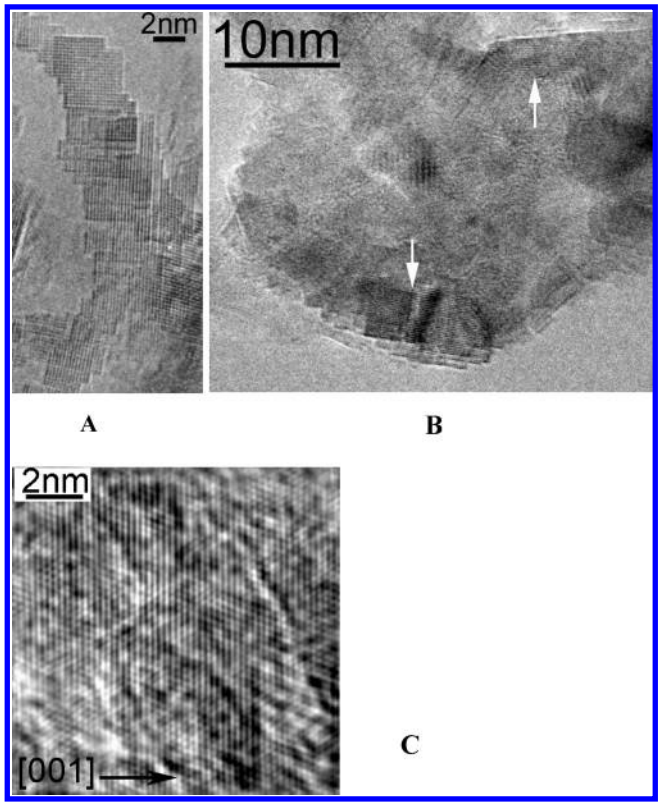

Figure 6. High-resolution TEM of AP-MgO (A) before the reaction with CCl_2F_2; (B) after 20 min, approximately the halfway point of the induction period (the arrows indicate crystallites that have grown to approximately 10 nm); (C) after 40 min, near the end of the induction period (the arrow shows crystallographic direction [001]).

TABLE 1: Halogen/Magnesium Elemental Ratios Determined by EDX for MgO Samples during the Induction Period

20 min, wide beam		40 min, wide beam	
Cl/Mg ratio	F/Mg ratio	Cl/Mg ratio	F/Mg ratio
0.7%	0.78%	1.2%	3.0%
0.7%	1.0%	1.4%	3.1%
20 min, narrow beam		**40 min, narrow beam**	
Cl/Mg ratio	F/Mg ratio	Cl/Mg ratio	F/Mg ratio
0.2%	4.9%	0.6%	65.1%

ingly, the EDX spectra of the larger particles in Figure 7 indicate that they consist of nearly pure MgF_2 with only a very small portion of oxygen. This observation agrees well with much greater width of diffraction peaks corresponding to the MgO in comparison with those of MgF_2 (Figure 8A). This indicates that the MgO crystallites are significantly smaller that the MgF_2 ones, in agreement with the EDX data. After the reaction, the large particles do not contain chlorine while some chorine is still present in the small particles. It appears that when the formation of bulk MgF_2 takes place, several small initial particles merge to form a larger particle, and both chlorine and oxygen atoms are substituted with fluorine.

The particle-size difference in the TEM image of the final sample is due to the difference in the transformation degree of the particles. Figure 5C shows a picture just prior to the fast transformation to MgF_2. Clusters, nearly 50 nm in size, are very closely packed to form a large agglomerate. Since the conversion of MgO to MgF_2 is exothermic, the clusters are heated during the fast part of the reaction allowing sintering of the whole agglomerate. The 50-nm particles remaining after the reaction

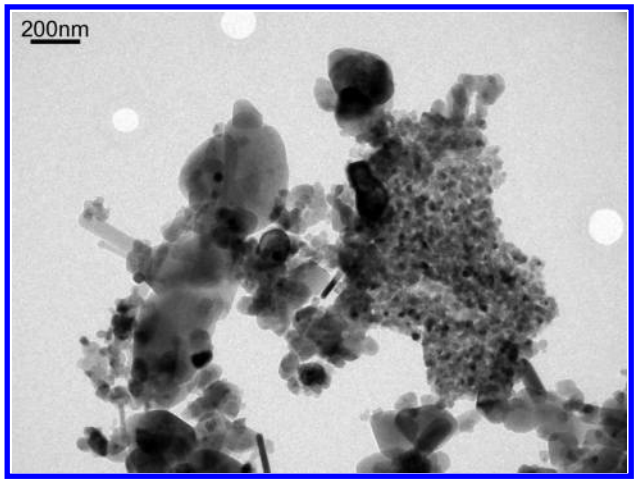

Figure 7. TEM image of AP-MgO after the reaction with CCl_2F_2 showing crystals of two typical size ranges: 200−400 nm and 40−50 nm.

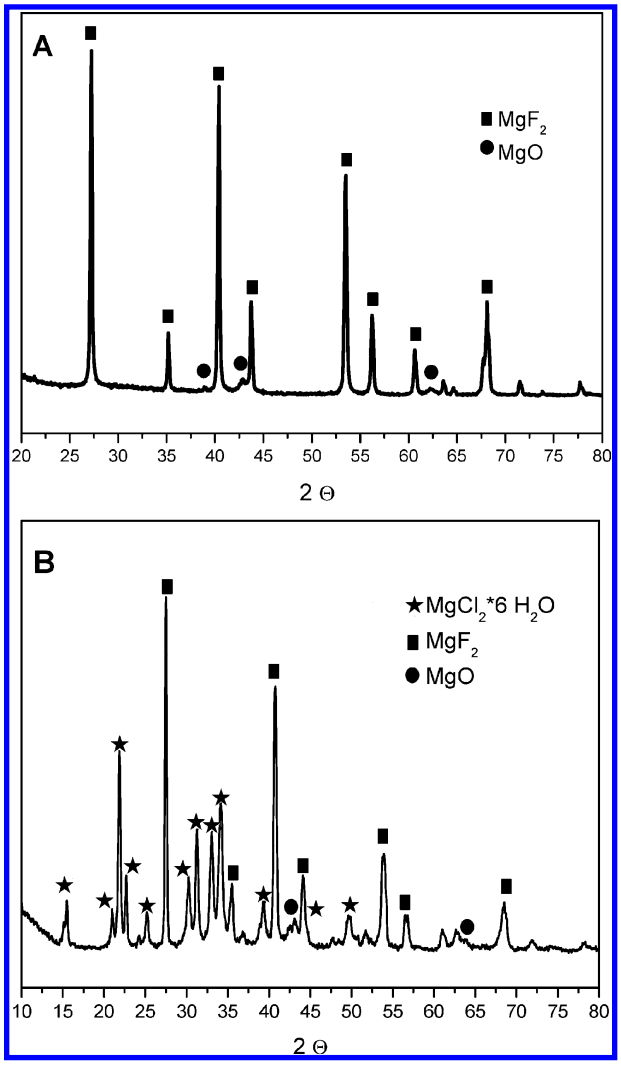

Figure 8. XRD patterns of samples after completion of the MgO reaction with CCl_2F_2. (A) Sample after reaction at 350 °C in a flow reactor showing MgF_2 and trace amounts of MgO crystals. Note the absence of $MgCl_2$ crystals. (B) Sample after reaction in a static reactor at 450 °C and MgO/CF_2Cl_2 ratio 2.5:1. All three crystalline phases are clearly seen.

are not as closely packed and did not react as much. Therefore, not enough heat was involved to cause sintering.

(b) Textural Studies. Surface areas of AP-MgO samples after reaction with CF_2Cl_2 are presented in Table 2. In all cases, the

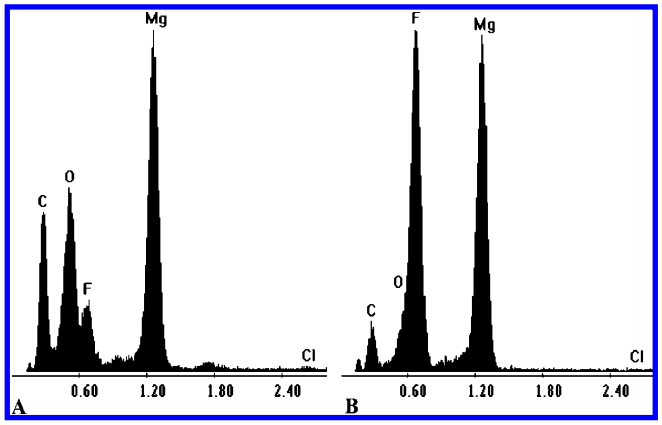

Figure 9. EDX spectra of MgO after reaction with CCl_2F_2, (a) cluster of small 40−50 nm particles, and (b) large particles.

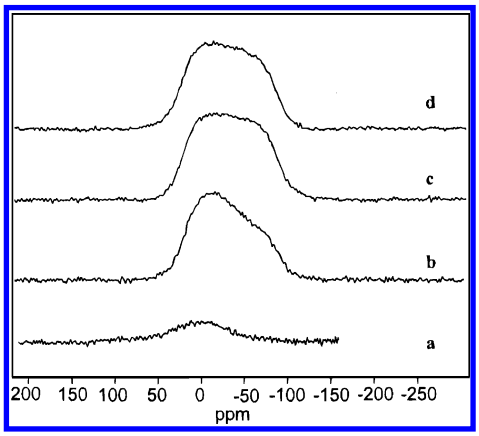

Figure 10. ^{19}F NMR spectra of AP-MgO samples after reaction with CF_2Cl_2 at 350 °C for 1 h (a) and 2 h 10 min (b), at 400 °C (c), and bulk MgF_2 (d).

TABLE 2: Specific Surface Areas and Weight Gains of AP-MgO Subjected to Reaction with CF_2Cl_2 at Different Temperatures or for Different Time

T, °C	weight gain, %	S.A., m^2/g
22	0	385
350	2.5	77
350	12.5	19
350	39	15
400	45	11
450	43.5	9
500	39	6

surface areas of the samples after reaction are significantly lower than that of the initial AP-MgO (380 m^2/g). This is due to intense sintering of both the initial magnesium oxide and resulting magnesium fluoride. The surface area of the sample with the weight gain of only 2.5% after reaction at 350 °C is already as low as 77 m^2/g. As shown in Table 2, the sintering of MgF_2 becomes more intense as the reaction temperature grows, resulting in very low values of the surface area (<10 m^2/g).

(c) NMR Study of MgO after Reaction with CF_2Cl_2. Figure 10 shows the ^{19}F NMR spectra of the AP-MgO samples fluorinated in the reaction with CF_2Cl_2. The spectra were registered (a) 1 h after beginning the experiment at 350 °C, which is middle of the induction period, (b) 10 min after the end of the induction period at 350 °C, and (c) after the reaction at 400 °C. The ^{19}F NMR spectrum of commercial magnesium fluoride is presented for comparison (d).

The spectra at the end of the reaction are very similar to that of commercial MgF_2 and are characterized by a broad resonance signal with anisotropy of about 60−70 ppm. For the sample during the fast transformation of MgO to MgF_2, spectrum b, the ^{19}F NMR line shape slightly differs from that of pure MgF_2 and can be described by a superposition of two lines: the signal of MgF_2 and a weak signal centered at about 0 ppm. Importantly, the ^{19}F signal at 0 ppm is also present in the sample during the induction period. It is not possible to unambiguously assign the weak signal to any of the known fluorine compounds. However, one may expect it to correspond to surface fluorine compounds, where F atoms do not possess a regular symmetric environment. This is in agreement with EDX results which clearly indicate the presence of magnesium fluoride species.

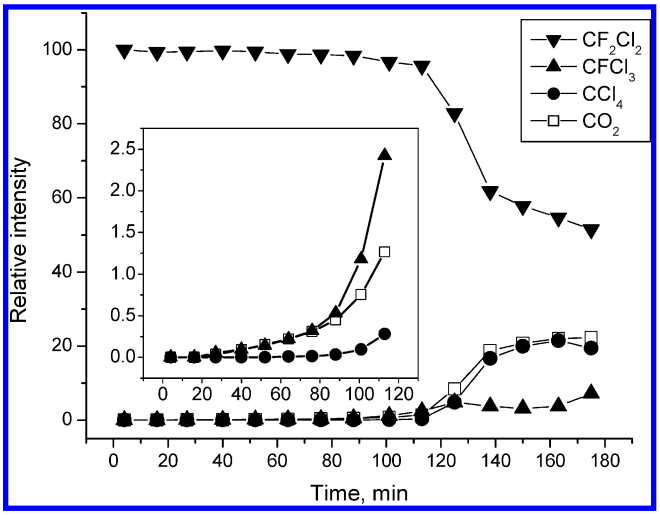

Figure 11. Relative intensities of main compounds present in the gas phase in a static reactor during the reaction of AP-MgO with CF_2Cl_2 at 340 °C. Inset shows in larger scale the composition of products formed during the induction period.

(d) GC-MS and FTIR Analysis of Products Formed in CF_2Cl_2 Reaction with MgO. Further evidence of the chemical transformations on the MgO surface to form halogenated species was obtained by GC-MS analysis of the products during the induction period. Such experiments were performed in a static reactor with the analysis of the gas phase by the GC-MS technique. The induction period phenomenon and dependence of its duration on the reaction temperature and type of MgO observed in the flow reactor were reproduced in the static reactor as well. The shortest induction period was again observed over AP-MgO, and it could be made longer by decreasing the reaction temperature.

The results obtained at 340 °C over AP-MgO activated at 500 °C are presented in Figure 11. The values along the ordinate axis are relative molar concentrations of the main gaseous compounds observed in the system, with the initial concentration of CF_2Cl_2 arbitrarily set to 100. This reaction temperature was selected on the basis of earlier experiments as in this case the induction period was long enough to distinguish the products formed at different stages. The carbon balance was maintained fairly well in the course of the reaction.

The main products formed during the induction period and after its completion are different. During the first 90 min when CF_2Cl_2 conversion was low, CO_2 and $CFCl_3$ formed in approximately 1:1 ratio were the main products. The amount of CCl_4 remained very low—either below the detection limit or just above it—and trailed the amounts of CO_2 and $CFCl_3$ at least by a factor of 20. No other gaseous products were registered.

The ratio between the products observed at this stage seems to indicate that significant chlorination of the MgO surface

occurs during the induction period in addition to the formation of surface magnesium fluoride. Most likely, two independent or quasi-independent reactions 1 and 6 take place.

$$2CF_2Cl_2 + MgCl_2 \rightarrow 2CFCl_3 + MgF_2 \quad (6)$$

As the actual amount of $CFCl_3$ formed in the reaction is approximately two times lower than that required for complete conversion of the hypothetic $MgCl_2$ intermediate, chlorinated species must be accumulated on the surface during the induction period. The ratio of products formed under static conditions suggests that gradual accumulation of chlorinated species takes place during the induction period according to overall reaction 7.

$$4CF_2Cl_2 + 4MgO \rightarrow 2CO_2 + 2CFCl_3 + MgCl_2 + 3MgF_2 \quad (7)$$

EDX data reported above prove the accumulation of chlorinated species in the flow conditions as well. Their exact structure remains unknown. Crystalline $MgCl_2$ was not observed among the solid products unless MgO was taken in excess. Most likely these are defective oxyhalide structures with variable amounts of halogen atoms partially substituting oxygen atoms of MgO and molecularly dispersed species with chlorine atoms substituting oxygen and fluorine atoms in an irregular manner in the MgO and MgF_2 structures, respectively. Their formation is likely to lead to the disordering of surface MgF_2 and hinder the formation of the bulk phase causing the induction period.

As the concentration of chloride grows, more and more $CFCl_3$ and CCl_4 are formed. The formation of defective oxyhalides and incorporation of halide atoms into the MgO structure also might increase the mobility of O^{2-} ions accelerating the ion exchange. This gradually leads to the end of the induction period and transition of the process to the second stage. Chlorine can be easily exchanged for fluorine in an exothermal process. At some point, this reaction may lead to autocatalytic heating that accelerates further fluorination of the oxide, which is also exothermal.

At the second stage (period between 110 and 140 min), the CF_2Cl_2 conversion rate grows considerably. Now the main products are CO_2 and CCl_4 formed in approximately 1:1 ratio. This ratio indicates that all $MgCl_2$ formed in reaction 1 is now completely converted to MgF_2 in reaction 8 leading to overall reaction 4.

$$CF_2Cl_2 + MgCl_2 \rightarrow CCl_4 + MgF_2 \quad (8)$$

Meanwhile, the amount of $CFCl_3$ does not change much at this stage. Still, it may serve as an intermediate in reaction 8, as an independent experiment has shown it to react with MgO under these conditions much easier than the initial CF_2Cl_2. The only other compound observed in the gas phase during this stage was CCl_2O present in a very low concentration (<0.1%).

The second stage of the process is relatively fast and is over when most MgO is converted to MgF_2. The MgO conversion degree estimated from CF_2Cl_2 conversion is close to 80%, which is in very good agreement with the above data obtained by the gravimetric technique in a flow reactor.

The exact composition of the reaction products was affected by the halocarbon/ MgO ratio, temperature, and pressure. Still, CCl_4 and $CFCl_3$ were always the main products formed in excess of the halocarbon. $CClF_3$, CCl_2O, and various C_2 halocarbons were the byproducts detected in small amounts in some experiments.

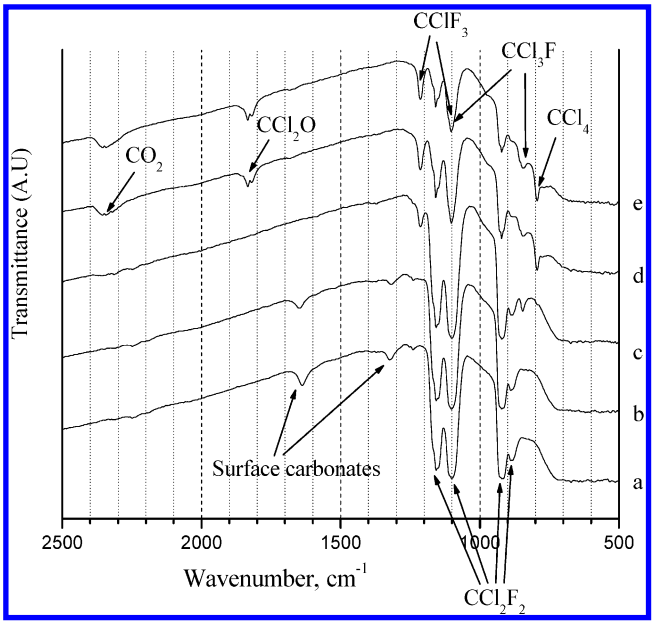

Figure 12. In-situ FTIR spectra registered during the reaction of AP-MgO with CF_2Cl_2 at 350 °C immediately after the halocarbon addition (a), and in 20 min (b), 40 min (c), 60 min (d), and 80 min (e). The most characteristic peaks corresponding to the main components present in the system are marked with arrows.

The above thermodynamic calculations suggest that an MgO excess is required to convert all CF_2Cl_2 to CO_2 and solid products. Indeed, we managed to achieve complete CF_2Cl_2 mineralization at 450 °C and MgO/CF_2Cl_2 ratio 2.5:1. The XRD spectrum of the solid sample after reaction shown in Figure 8B indicates the presence of both MgF_2 and $MgCl_2 \cdot 6\ H_2O$ in addition to unreacted MgO. Magnesium chloride is observed in the form of the crystalline hydrate due to fast hydration of $MgCl_2$ after the sample is taken from the reactor to the atmosphere.

These results were confirmed by in-situ FTIR experiments. Spectra obtained in a representative experiment are presented in Figure 12. No major changes in the IR spectrum were observed during the induction period (first 20 min). The spectrum recorded in 40 min after the CF_2Cl_2 introduction (spectrum c) corresponds to an intermediate state when surface carbonates (peaks at 1639 and 1324 cm^{-1}) are gone, while new peaks start to appear at 1214 cm^{-1} ($CClF_3$) and 845 cm^{-1} ($CFCl_3$). Just 20 min later, the reaction is mostly over, with characteristic lines of CCl_4, CCl_2O, and CO_2 appearing in the spectrum and the amount of CF_2Cl_2 decreasing considerably (spectrum d). No significant changes in the IR spectrum were observed in the following 20 min.

The peaks corresponding to isolated surface hydroxyl groups (3725 cm^{-1}) and surface carbonates are the only ones reliably attributed to the solid phase. All the other peaks were present in the spectrum corresponding to the gas phase and quickly disappeared when the sample was evacuated at 350 °C. Another important result is the lack of the CO signal that could not be easily quantified by the GC-MS technique in the presence of CO_2. As it has never been observed in the FTIR experiments, we are able to conclude that it is formed only in very small amounts, if at all.

Conclusions

Nanocrystalline MgO appears to be an effective destructive sorbent for decomposition of CF_2Cl_2 (halocarbon-12). The reaction taking place at temperatures as low as 325 °C is

characterized by a pronounced induction period that can be several hours long. The kinetics and the overall depth of the CF_2Cl_2 reaction with MgO have been found to depend significantly on the sample morphology. The reaction appears to be structurally sensitive as shown by comparison of the reactivity of MgO samples prepared by different techniques. Nanocrystalline AP-MgO samples are characterized by the highest reactivity, minimum induction period, and maximum conversion.

Apparently, the induction period corresponds to the time necessary for gradual accumulation of structural defects on the surface and near-surface region of MgO, which are required for the subsequent reaction in the bulk. Although the exact nature of these changes is not completely understood thus far, it seems quite logical that smaller and more defective aerogel particles are more susceptible to them, while the reaction is limited to the surface for large crystallites of commercial MgO.

NMR and GC-MS data further support that the formation of Mg−X on the surface and in the bulk of the MgO nanocrystals is needed for the reaction to progress. The formation of defective oxyhalides and incorporation of halide atoms into the MgO structure, most likely, increases the mobility of O^{2-} ions accelerating the ion exchange. This effect seems to be similar to that of the addition of transition metal oxides that were earlier found to allow AP-MgO to react with carbon tertrachloride faster and deeper.[8] In that case, it was suggested that the formation of chlorides of the corresponding transition metals made the nanoparticles more mobile, thus, encouraging further Cl^-/O^{2-} exchange.

We believe that further investigation of textural, structural, and chemical changes taking place during the induction period and right after it will significantly deepen our knowledge of the mechanisms of topochemical transformation at the nanoparticle scale and make it possible to synthesize better, more efficient destructive sorbents which are able to function at lower temperatures.

Acknowledgment. The financial support of the US Army Research office, CRDF (Project RC1-2340-NO-02), Presidium of the Russian Academy of Sciences (Project 8.23), and Russian Department of Industry and Science (Projects SS-2120.2003.3 and SS-1140.2003.3) is acknowledged with gratitude.

References and Notes

(1) Wolf, G. In *Encyclopedia of Chemical Technology*; Kroschwitz, J I., Howe, G., Eds.; Wiley: New York, 1994; Vol. 1, p 715.
(2) Rowland, M. J.; Molina, F. S. *Nature* **1974**, *249*, 810.
(3) Takita, Y.; Li, G.-L.; Matsuzaki, R.; Wakamatsu, H.; Nishiguchi, H.; Moroka, Y.; Ishihar, T. *Chem. Lett*. **1997**, 13.
(4) Karmakar, S.; Greene, H. L. *J. Catal.* **1995**, *151*, 394.
(5) Xianzhi, F.; Zeltner, W. A.; Yang, Q.; Anderson, M. A. *J. Catal*. **1997** *168*, 482.
(6) Stark, J. V.; Park, D. G.; Lagadic, I.; Klabunde, K. J. *Chem. Mater.* **1996**, *8*, 1904.
(7) Stark, J. V.; Klabunde, K. J. *Chem. Mater*. **1996**, *8*, 1913.
(8) Klabunde, K. J.; Stark, J. V.; Koper, O. B.; Mohs, C.; Park, D. G.; Decker, S.; Jiang, Y.; Lagadic, I.; Zhang, D. *J. Phys. Chem.* **1996**, *100*, 12142.
(9) Li, Y.-X.; Koper, O. B.; Atteya, M.; Klabunde, K. J. *Chem. Mater.* **1992**, *4*, 323.
(10) Graven, W. M.; Paton, J. D.; Weller, S. W. *Ind. Eng. Process Des. Dev*. **1966**, *5*, 34.
(11) Graven, W. M.; Weller, S. W.; Peters, D. L. *Ind. Eng. Process Des. Dev.* **1966**, *5*, 183.
(12) Li, Y.-X.; Schlup, J. R.; Klabunde, K. J. *Langmuir* **1991**, *7*, 1394.
(13) Koper, O. B.; Li, Y.-X.; Klabunde, K. J. *Chem. Mater.* **1993**, *5*, 500.
(14) Koper, O. B.; Klabunde, K. J. *Chem. Mater*. **1997**, *9*, 2481.
(15) Jiang, Y.; Decker, S.; Mohs, C.; Klabunde, K. J. *J. Catal.* **1998**, *180*, 24.
(16) Decker, S.; Klabunde, K. J. *J. Am. Chem. Soc*. **1996**, *118*, 12465.
(17) Decker, S.; Lagadic, I.; Klabunde, K. J.; Michalowicz, A.; Moscovici, J. *Chem. Mater*. **1998**, *10*, 674.
(18) Martyanov, I.; Klabunde, K. J. *J. Catal.* **2004**, *224*, 340.
(19) Tamai, T.; Inazu, K.; Aika, K. *Chem. Lett*. **2003**, 32.
(20) Itoh, H.; Utamapanya, S.; Stark, J. V.; Klabunde, K. J.; Schlup, J. R. *Chem. Mater.* **1993**, *5*, 71.
(21) Mishakov, I. V.; Bedilo, A. F.; Richards, R. M.; Chesnokov, V. V.; Volodin, A. M.; Zaikovskii, V. I.; Buyanov, R. A.; Klabunde, K. J. *J. Catal.* **2002**, *206*, 40.
(22) Basu, P.; Ballinger, T. H.; Yates, J. T. *Rev. Sci. Instrum.* **1988**, *59*, 1321.
(23) Koper, O. B.; Wovchko, E. A.; Glass, J. A.; Yates, J. T.; Klabunde, K. J. *Langmuir* **1995**, *11*, 2054.
(24) Richards, R.; Li, W.; Decker, S.; Davidson, C.; Koper, O.; Zaikovski, V.; Volodin, A.; Rieker, T.; Klabunde, K. J. *J. Am. Chem. Soc.* **2000**, *122*, 4921.